What explains the year-to-year variation in growing season timing of boreal black spruce forests?

Mariam El-Amine [1,a,b], Alexandre Roy[b,c], Franziska Koebsch[d], Jennifer L. Baltzer[e], Alan Barr[f], Andrew Black[g], Hiroki Ikawa[h], Hiroki Iwata[i], Hideki Kobayashi[j], Masahito Ueyama[k], and Oliver Sonnentag[a,b,l]

[a] Département de géographie, Université de Montréal, 1375 avenue Thérèse-Lavoie-Roux, Montréal, QC H2V 0B3, Canada

[b] Centre d'études nordiques, Université Laval, 2405 rue de la Terrasse, Québec, QC G1V 0A6, Canada

[c] Département des sciences de l'environnement, Université du Québec à Trois-Rivières, 3351 boulevard des Forges, Trois-Rivières, QC G8Z 4M3, Canada

[d] Bioclimatology, Faculty of Forest Sciences and Forest Ecology, University of Goettingen, Büsgenweg 2, 37077 Göttingen, Germany

[e] Department of Biology, Wilfrid Laurier University, 75 University Avenue West Waterloo, ON N2L 3C5, Canada

[f] Global Institute for Water Security, University of Saskatchewan, 11 Innovation Blvd., Saskatoon, SK S7N 3H5, Canada

[g] Faculty of Land and Food Systems, University of British Columbia, 2357 Main Mall, Vancouver, BC V6T 1Z4, Canada

[1] Corresponding Authors: mailto:mariam.el-amine@umontreal.ca; oliver.sonnentag@umontreal.ca

[h] Hokkaido Agricultural Research Center, National Agriculture and Food Research Organization, 1, Hitsujigaoka, Sapporo, Hokkaido, 062-8555, Japan

[i] Department of Environmental Science, Shinshu University, 3-1-1 Asahi, Matsumoto, Nagano 390-8621 Japan

[j] Institute of Arctic Climate and Environment Research, Japan Agency for Marine-Earth Science and Technology, 2-15, Natsushima-cho, Yokosuka-city, Kanagawa, 237-0061, Japan

[k] Graduate School of Life and Environmental Sciences, Osaka Prefecture University, 1-1 Gakuen-cho, Nakaku, Sakai, Osaka 599-8531, Japan

[l] Centre d'étude de la forêt, Université du Québec à Montréal, 141 Président-Kennedy, Montréal, QC H2X 1Y4, Canada

Under revision for publication in

Agricultural and Forest Meteorology

(April 2022)

Abstract

Amplified climate warming in high latitudes is expected to affect growing season timing of the vast boreal biome. It is unclear whether the presence of permafrost (perennially frozen ground) might have an influence on changes in growing season timing. This study examined how different environmental variables explained, either directly or indirectly, the variation in growing season timing of boreal forest stands with and without permafrost. We expected that environmental variables explaining the variation in growing season timing differed or had different explanatory power depending on permafrost presence or absence. The growing season was delineated from daily gross primary productivity (GPP) time series derived from 40 site-year data of net ecosystem carbon dioxide exchange measured with eddy covariance techniques over five black spruce (*Picea mariana* [Mill.])-dominated boreal forest stands in North America. In permafrost-free forest stands, a combination of start in canopy 'green-up' in spring and the timing of air and soil temperature increasing above freezing explained the start-of-season (SOS_{GPP}). Results from commonality analysis and structural equation modeling suggest that canopy 'green-up' and air temperature directly affected SOS_{GPP} in permafrost-free forest stands. In addition, soil temperature acted as mediator for an indirect effect of air temperature on SOS_{GPP}. In contrast, none of the environmental variables, or their combination, explained the variation in SOS_{GPP} in forest stands with permafrost. The explanatory power of environmental variables was more consistent regarding the end-of-season (EOS_{GPP}). In both, forest stands with and without permafrost, EOS_{GPP} was directly explained by mean soil water content in the fall and the first day of continuous snowpack formation. A better understanding how environmental

variables control SOS_{GPP} and EOS_{GPP} in forest stands with and without permafrost will help to refine parameterizations of the boreal biome in Earth system models.

Keywords

Carbon dioxide, photosynthesis, growing season, boreal forest, permafrost, eddy covariance

1. Introduction

As the largest biome in North America, boreal forests, lakes, and wetlands constitute integral components of the climate system, affecting atmospheric dynamics and greenhouse gas concentrations through land surface-atmosphere interactions. Coniferous tree species comprise between 60 % and 90 % of the boreal forest (Black *et al.*, 2004; Nilsson *et al.*, 2000). In North America, the most widespread coniferous tree species is black spruce (*Picea mariana* [Mill.]; Viereck and Johnston, 1990). About 80 % of the boreal forest is underlain by permafrost (Helbig *et al.*, 2016), defined as a ground layer at or below 0 °C for at least two years (Harris *et al.*, 1988).

The carbon balance of the boreal biome is strongly influenced by various environmental variables that control the process of photosynthetic carbon dioxide (CO_2) uptake. These controls include air and soil temperature (Barr *et al.*, 2009; Chen *et al.*, 2006; Krishnan *et al.*, 2008), water availability (Dunn *et al.*, 2007; Krishnan *et al.*, 2008) and radiation (Barr *et al.*, 2009; Krishnan *et al.*, 2008). The annual carbon source-sink strength is also influenced by the start and end of the growing season (Richardson *et al.*, 2013). For example, an extension of the growing

43 season caused by higher air temperature leads to enhanced annual photosynthetic CO_2 uptake, if
44 there are no other environmental limitations such as radiation or water and nutrient availability
45 (Richardson *et al.*, 2010). However, increased spring productivity might be counteracted by
46 increased ecosystem respiration and water stress later in the growing season (Buermann *et al.*,
47 2018; Piao *et al.*, 2008).

48 The growing season can be delineated from daily gross primary productivity (GPP) time
49 series derived from net ecosystem CO_2 exchange (NEE) measurements made with eddy
50 covariance techniques (Baldocchi and Meyers, 1998). Previous studies have found that higher air
51 temperature in spring stimulated an earlier start-of-season (SOS_{GPP}) in boreal forests (Suni *et al.*,
52 2003a; Ueyama *et al.*, 2014). More specifically, Barr *et al.* (2009) showed that SOS_{GPP} in boreal
53 forest stands corresponded with spring thaw, i.e., the period characterized by above-freezing air
54 temperature, soil thaw, and snowmelt, resulting in the availability of liquid water (Ahmed *et al.*,
55 2021). However, Suni *et al.* (2003b) showed that soil thaw was not complete until several weeks
56 after SOS_{GPP} and hence could not be considered as a trigger for photosynthetic recovery. Their
57 findings suggest that complete soil thaw is not necessary for trees to access liquid water and
58 initiate photosynthesis in the spring. Similarly, in a Rocky Mountain subalpine forest stand,
59 Bowling *et al.* (2018) observed that photosynthesis occurred in early spring while there was no
60 apparent sap flow, suggesting that water transport from the soil was not initially necessary for
61 photosynthetic recovery. Suni *et al.* (2003b) and Bowling *et al.* (2018) concluded that water
62 stored in stems over winter was sufficient for photosynthetic recovery with above-freezing air
63 temperature. Also, in a boreal forest stand in interior Alaska, Parazoo *et al.* (2018) showed that
64 soil thaw started before or coincided with SOS_{GPP}. Initiation of snowmelt was also associated

65 with SOS_{GPP}, although complete snowpack disappearance was not necessary for photosynthetic
66 recovery (Arneth *et al.*, 2006; Pulliainen *et al.*, 2017).

67 The end-of-season (EOS_{GPP}) has received much less attention than SOS_{GPP}, but the
68 importance of below-freezing air temperature (Barr *et al.*, 2009) and photoperiod (i.e., day
69 length; Way and Montgomery, 2015) was demonstrated. However, photoperiod is a function of
70 latitude and time-of-year and as such does not account for the variation EOS_{GPP} observed in
71 specific locations (Way and Montgomery, 2015). In short, no single environmental variable
72 directly explains the variation in either SOS_{GPP} or EOS_{GPP} across the boreal forest. Additional
73 complexity is added through the interplay of environmental variables (Suni *et al.*, 2003b). For
74 example, temperature affects photosynthetic CO_2 uptake in two ways: directly by regulating the
75 underlying thermodynamic enzyme reactions and indirectly as a control factor for seasonal
76 vegetation dynamics (Koebsch *et al.*, 2020; Ueyama *et al.*, 2014). Such indirect effects were
77 previously termed as 'mediation effects' (Baron and Kenny, 1986).

78 Vegetation canopy development and biochemistry (e.g., budburst, senescence, changes in
79 chlorophyll concentration, even though modest in evergreen taxa, and changes in xanthophyll
80 cycle carotenoid concentration; e.g., Delpierre *et al.*, 2016; Öquist and Huner, 2003; Ensminger
81 *et al.*, 2004; Walter-McNeill *et al.*, 2021) follow a seasonal, 'phenological', cycle (Richardson *et*
82 *al.*, 2013). Phenology can be tracked with spectral vegetation indices indicating canopy
83 'greenness'. Examples include the widely used normalized difference vegetation index (NDVI;
84 Tucker, 1979). However, the evergreen foliage of coniferous taxa such as spruce hampers the use
85 of NDVI to track subtle phenological changes compared to deciduous broad-leaved and
86 coniferous taxa (e.g., Jönsson *et al.*, 2010; Wang *et al.*, 2017; Magney *et al.,* 2019). Snow cover

poses an additional challenge to track phenology in the boreal biome by strongly affecting the spectral reflectance of the landscape (Jin *et al.*, 2017). Based on thorough theoretical considerations, the plant phenology index (PPI) was proposed to address these two challenges (Jin and Eklundh, 2014), thus offering a promising alternative to NDVI to track phenology of coniferous evergreen boreal forest stands.

Ongoing climate change will affect growing season timing, thus influencing the CO_2 sink-source strength of ecosystems. Environmental conditions in the boreal biome are, at least partially, controlled by the presence of permafrost (e.g., Quinton *et al.*, 2019; Shur and Jorgenson, 2007). Thus, differences in how environmental variables control variability in SOS_{GPP} and EOS_{GPP} are to be expected across the boreal biome, even among populations of the same species (reviewed in Reich, 2014). For example, trees at higher latitudes are exposed to harsher climate and environmental conditions and therefore might have more resource-conservative life history strategies, including reduced plasticity, compared to more southerly populations (e.g., Sniderhan *et al.*, 2018). Hence, high-latitude populations of a given species may be less responsive to changes in environmental variables compared to their southern counterparts because the former are more reliant on non-varying cues, such as photoperiod.

Here, we examined how environmental variables, either directly or indirectly, control SOS_{GPP} and EOS_{GPP} in five black spruce-dominated boreal forest stands. This study was based on 40 site-years of eddy covariance data and supporting measurements, analyzed in a statistical framework that includes commonality analysis and structural equation modeling (Koebsch *et al.*, 2020). Distinguishing between permafrost-free forest stands and those where permafrost is present, this

study aimed to explain the year-to-year variation in growing season timing, i.e., SOS_{GPP} and EOS_{GPP}, of boreal black spruce forests in North America.

2. Material and methods

2.1 Gross primary productivity

The study sites were five black spruce-dominated forest stands in the boreal biome of North America. Collectively, these forest stands span a wide range of climate, environmental and permafrost conditions (Figure 1, Table 1, Supplement S1). The permafrost-free forest stands included 'Quebec – Eastern Boreal, Mature Black Spruce' (CA-Qfo) and 'Saskatchewan – Western Boreal, Mature Black Spruce' (CA-Obs). The forest stands where permafrost is present were 'Scotty Creek Landscape' (CA-SCC), 'University of Alaska, Fairbanks' (US-Uaf) and 'Poker Flat Research Range Black Spruce Forest' (US-Prr). The understory and ground cover vegetation at all five forest stands comprises characteristic shrubs (e.g., *Rhododendron groenlandicum*, *Betula* and *Salix* species) and a mixture of mosses (*Sphagnum* and feather mosses, among others) and lichens (notably, *Cladina* spp.), respectively.

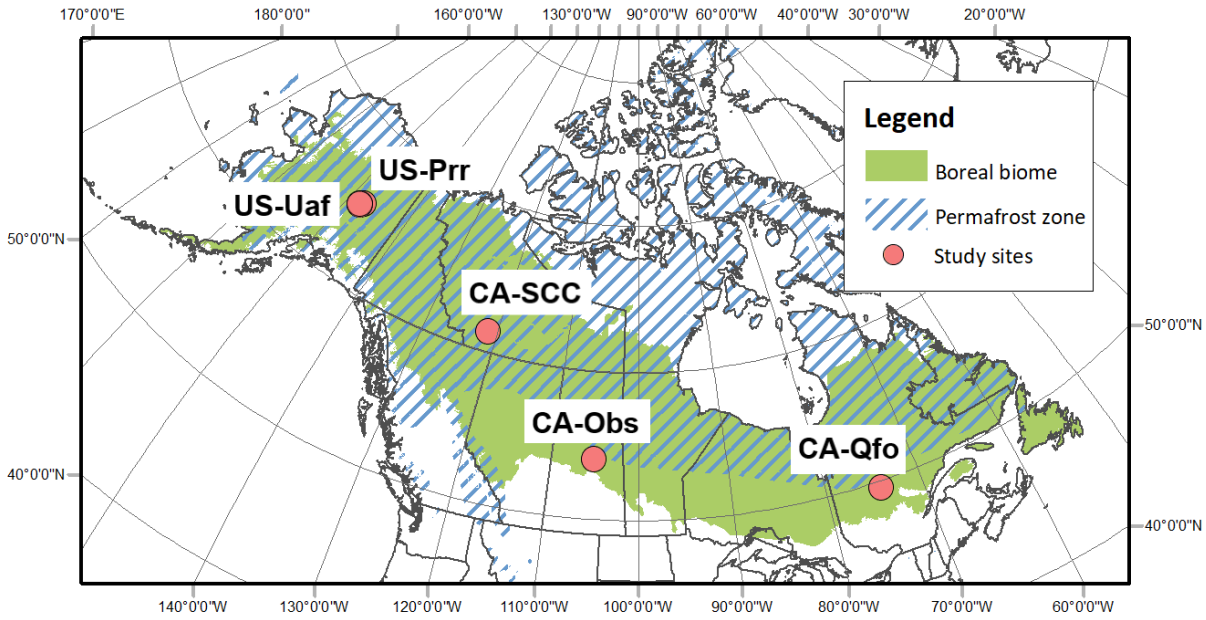

Figure 1: Location of the study sites. All sites are black spruce-dominated forest stands and their location within the boreal biome and the permafrost zone of North America are depicted. US-Uaf: 'University of Alaska, Fairbanks'; Us-Prr: 'Poker Flat Research Range Black Spruce Forest'; CA-SCC: 'Scotty Creek Landscape'; CA-Obs: 'Saskatchewan Western Boreal, Mature Black Spruce'; CA-Qfo: 'Quebec – Eastern Boreal, Mature Black Spruce'. North America map: U.S. Geological Survey (Commission for Environmental Cooperation, 2011); boreal biome: Natural Resources Canada (Brandt, 2009); permafrost zone: National Snow & Ice Data Center (Brown *et al.*, 2002).

Site name (AmeriFlux-ID)	Latitude, longitude	MATa (°C)	PPT (mm)	LAI (m^2/m^2)	Permafrost areal extent	Years of observations	Source
Quebec -Eastern Boreal, Mature Black Spruce (CA-Qfo)[1]	49.49°N, 74.34°W	-0.36	962	3.7 (mean annual value)	Absent	2004-2009 [2009]	FLUXNET
Saskatchewan - Western Boreal, Mature Black Spruce (CA-Obs)[1,2]	53.99°N, 105.12°W	0.79	406	3.8 (mean annual value)	Absent	2000-2015 [2000; 2012]	Global Institute for Water Security (University of Saskatchewan)*
Scotty Creek Landscape (CA-SCC)[3,4]	61.31°N, 121.30°W	-2.8	388	0.61 (mid-summer value)	Sporadic	2014-2018	AmeriFlux
University of Alaska, Fairbanks (US-Uaf)[5]	64.87°N, 147.86°W	-2.9	263	1.8 (mid-summer value)	Discontinuous	2003-2018 [2003-2006]	AmeriFlux
Poker Flat Research Range Black Spruce Forest (US-Prr)[6,7]	65.12°N, 147.49°W	-2.0	275	1.51 (maximum annual value)	Discontinuous	2011-2016 [2011; 2013]	AmeriFlux

[1]Bergeron *et al.* (2007), [2]Barr *et al.* (2006), [3]Helbig *et al.* (2017), [4]Warren *et al.* (2018), [5]Ueyama *et al.* (2014), [6]Ikawa *et al.* (2015), [7]Kobayashi *et al.* (2016)
* The data from CA-Obs are also available in FLUXNET and AmeriFlux, but only until 2010.

Table 1: Study site descriptions. MATa: mean annual air temperature; PPT: annual precipitation; LAI: leaf area index. Permafrost areal extent is absent (0 %), isolated patches (>0-10 %), sporadic (>10-50 %), discontinuous (>50-90 %), and continuous (>90-100 %) based on data provided by Gruber (2012). The presence of permafrost at CA-SCC, US-Uaf and US-Prr was confirmed by site investigators (*personal communication*). Square brackets in years of observations indicate the years that were excluded from the analyses, because either the flux, meteorological or spectral vegetation index data were not available.

129 Due to data availability, the dataset used in this study was limited to 40 site-year data of daily
130 NEE-derived GPP and supporting measurements (Supplement S1). Details on eddy covariance
131 data collection and processing, including gap-filling and flux partitioning of NEE into GPP and
132 ecosystem respiration, can be found in Barr *et al.* (2004) for CA-Qfo and CA-Obs, in Reichstein
133 *et al.* (2005) and Runkle *et al.* (2013) for CA-SCC, in Ikawa *et al.* (2015) and Reichstein *et al.*
134 (2005) for US-Prr, and Ueyama *et al.* (2014) for US-Uaf. For each site-year, day-of-year (DOY)
135 representing SOS_{GPP} and EOS_{GPP} was determined by fitting a double-logistic function to the daily
136 GPP time series (Gonsamo *et al,* 2013). The first maximum and the last minimum of the third
137 derivative of the fitted curve were used to define SOS_{GPP} and EOS_{GPP}, respectively (Figure 2a).

138

139 **2.2 Environmental variables**

140 The environmental variables included in this study were above-canopy air temperature (Ta),
141 near-surface soil temperature (Ts), soil water content (SWC), and photosynthetically active
142 radiation (PAR) measured as photosynthetic photon flux density (Supplement S1). Soil
143 temperature was consistently measured at a depth of 5 cm, except for US-Uaf where it was
144 measured at a depth of 10 cm. There was no statistically significant difference in the strength of
145 the correlations between year-to-year anomalies (Δ) in the timing of soil thaw in spring (ΔSOS_{Ts})
146 and SOS_{GPP} (ΔSOS_{GPP}) or between the timing of soil freeze in fall (ΔEOS_{Ts}) and EOS_{GPP}
147 (ΔEOS_{GPP}) due this difference in near-surface Ts measurement depth (Supplement 2). The plant
148 phenology index (PPI; Jin and Eklundh, 2014) was determined using the Moderate Resolution
149 Imaging Spectroradiometer (MODIS) MCD43A4 Nadir Bidirectional Reflectance Distribution
150 Function-Adjusted Reflectance product with 500-m spatial resolution (Appendix A; ORNL
151 DAAC, 2018; Schaaf and Wang, 2015). Snowpack presence data were obtained from the

National Oceanic and Atmospheric Administration interactive multi-sensor snow and ice mapping system with 1-km spatial resolution (U.S. National Ice Center, 2008).

For each site-year, the DOY representing the start-of-season (SOS) and end-of-season (EOS) was determined for each environmental variable, except for SWC and PAR (Figure 2, Table 2, Supplement S3). A double-logistic function was fitted to the daily PPI time series (Gonsamo *et al.*, 2013; Jin *et al.*, 2017; Wu *et al.*, 2017). The first maximum and last minimum of the third derivative of the fitted curve were used to delineate the start of canopy 'green-up' (SOS_{PPI}) and the end of canopy 'green-down' (EOS_{PPI}), respectively (Figure 2b). Inspired by Barr *et al.* (2009), the timing of Ta increasing above freezing in spring (SOS_{Ta}) and decreasing below freezing in fall (EOS_{Ta}) was delineated when the cumulative Ta reached a minimum in spring and a maximum in fall (Figure 2c). The timing in Ts indicating soil thaw in spring (SOS_{Ts}) and freezing in fall (EOS_{Ts}) was estimated accordingly (Figure 2d). This simple approach ignores that liquid pore water might be present at Ts < 0 °C due to pore water solutes (Edwards and Cresser 1992). The start of the snow-free period (SOS_{Snow}) was defined by the first DOY when the ground was snow-free for 13 days in a 14-day period (Figures 2c and d; Brown and Mote, 2009). Similarly, the end of the snow-free period (EOS_{Snow}) was defined by the first DOY when the ground was continuously covered by snow for 13 days in a 14-day period (Figures 2c and d). These definitions were chosen to avoid a premature or delayed start or end of the snow-free period, as short but temporary snowmelt or snowpack formation events can occur in spring and fall. For PAR and SWC, early season (March to May; $\overline{PAR_{MAM}}$ and $\overline{SWC_{MAM}}$) and late season averages (July to October; $\overline{PAR_{JASO}}$ and $\overline{SWC_{JASO}}$) were calculated instead of delineating a DOY representing an arbitrary start or end of the season. The averages of SWC were calculated after

removing the days when the soil was below 0°C, since the dielectric measurements made with soil moisture probes respond to ice formation in the soil (Roy *et al.*, 2020).

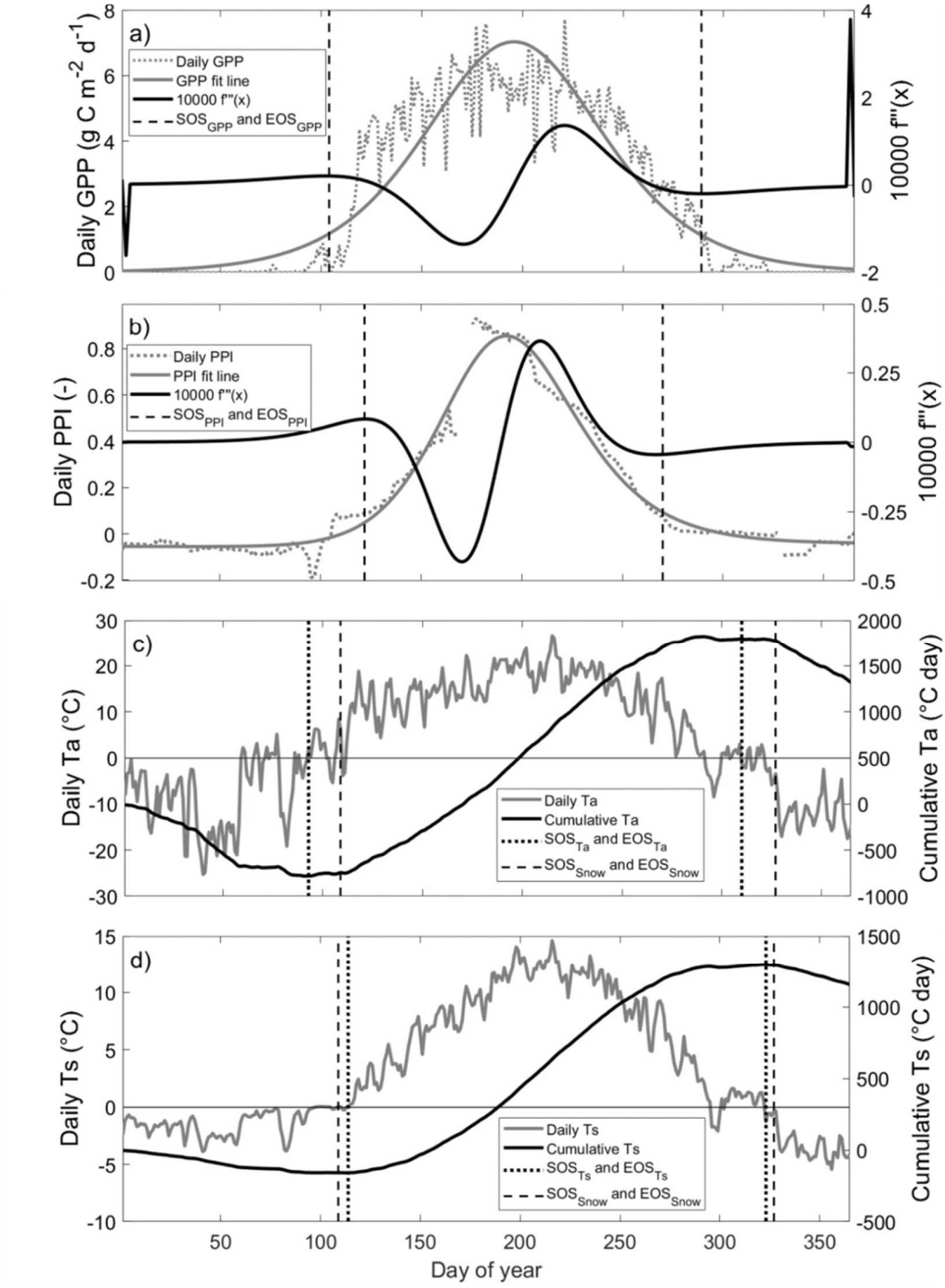

Figure 2: Daily observed and fitted (a) gross primary productivity (GPP) and (b) plant phenology index (PPI) at 'Saskatchewan - Western Boreal, Mature Black Spruce' (CA-Obs) in 2001, and

third derivative of the fitted function ($f'''(x)$), for which the scale is enhanced for visual clarity (x 10000). Daily observed and cumulative (c) air temperature (Ta) and (d) soil temperature (Ts) at CA-Obs in 2001. SOS: start-of-season; EOS: end-of-season; SOS_{Snow}: start of the snow-free period; EOS_{Snow}: end of the snow-free period.

Variable of interest	**Biological interpretation**	**Computation**
Start-of-season in spring (SOS_{GPP}) and end-of-season in fall (EOS_{GPP}) delineated from daily GPP	Photosynthetic recovery in spring and cessation in fall (Gonsamo *et al.*, 2013)	DOY corresponding to the first maximum (last minimum) of the third derivative of a fitted double-logistic function fitted to daily GPP
Controls	**Mechanisms**	
Canopy 'green-up' in spring (SOS_{PPI}) and end of 'green-down' in fall (EOS_{PPI})	Vegetation canopy 'greenness' indicating canopy development and biochemistry (Wang *et al.*, 2017)	DOY corresponding to the first maximum (last minimum) of the third derivative of a fitted double-logistic function of the observed PPI
Timing of Ta increasing above freezing in spring (SOS_{Ta}) and decreasing below freezing in fall (EOS_{Ts})	Temperature-dependence of chemical reactions involved in the Calvin cycle (Badeck *et al.*, 2004)	DOY when the cumulative Ta reaches a minimum (maximum)
Timing of soil thaw in spring (SOS_{Ts}) and freeze in fall (EOS_{Ts})	Soil thaw renders water in the soil available in liquid form (Barr *et al.*, 2009)	DOY when the cumulative Ts reaches a minimum (maximum)
Start (SOS_{Snow}) and end (EOS_{Snow}) of the snow-free period	Influence on Ts and SWC: snowmelt supplies the soil with water in spring and snow cover provides an insulation layer in the fall (Lawrence and Slater, 2010)	DOY when the ground is snow-free in spring (covered by snow in fall) for 13 days in a 14-day period
Early and late growing season PAR ($\overline{PAR_{MAM}}$ and $\overline{PAR_{JASO}}$)	Influence on Ta, Ts and on total available radiation for photosynthesis (Way and Montgomery, 2015)	Average of PAR from March to May (July to October)

Early and late growing season SWC ($\overline{SWC_{MAM}}$ and $\overline{SWC_{JASO}}$)	Soil water availability affects the opening and closing of stomata, which in turn affects the uptake of CO_2 by vegetation (Anderson, 1936; Reich *et al.*, 2018)	March to May (July to October), excluding days when the soil was below 0°C

Table 2: Delineation of start-of-season (SOS) and end-of-season (EOS). GPP: gross primary productivity; PPI: plant phenology index; Ta: air temperature; Ts: soil temperature; DOY: day-of-year; PAR: photosynthetically active radiation; SWC: soil water content; MAM: March-April-May; JASO: July-August-September-October.

176

177 **2.3 Statistical analyses**

178 The statistical analyses were conducted on year-to-year anomalies (Δ) in SOS_{GPP} (ΔSOS_{GPP}),
179 EOS_{GPP} (ΔEOS_{GPP}) and environmental variables (i.e., deviation from the multi-year mean DOY
180 or early- and late-season averages). Because the number of site-year data varied among sites, the
181 anomalies were calculated for each site individually. Using time anomalies rather than DOYs
182 allowed comparisons among forest stands by centering the data around their multi-year means to
183 understand the causes of variation in SOS_{GPP} and EOS_{GPP}.

184 Separate analyses were conducted for the SOS and EOS, and each of these analyses was
185 conducted separately for sites with and without permafrost. As an exploratory method, pairwise
186 correlations (Pearson correlation coefficient, r) were calculated between ΔSOS_{GPP} (ΔEOS_{GPP}) and
187 the anomalies of the SOS (EOS) of the environmental variables. Variables that had a significant
188 correlation with ΔSOS_{GPP} or ΔEOS_{GPP}, either at sites with or without permafrost, were kept for
189 further statistical analyses. Statistical significance was set at $\alpha = 0.05$ for all analyses.

190 Pairwise correlations provide only limited insights into the mechanisms at stake. The multi-
191 faceted interaction between environmental variables needs to be considered. Above all, pairwise
192 correlation cannot account for third-variable effects such as mediation (i.e., a control variable

exerts an indirect effect on an outcome variable by influencing a third variable, which in turn impacts the outcome variable; Alwin and Hauser, 1975). Here, we used commonality analysis to gain insights on possible mediation effects.

Commonality analysis (CA; Mood, 1969; Newton and Spurrell, 1967; Ray-Mukherjee *et al.*, 2014) partitions the explained variation of a dependent variable to multiple independent variables, and thereby specifies whether a variable exerts its effect individually (as a unique effect) or in combination with other, intercorrelated, variables (as a common effect). In contrast to multiple linear regression, the interpretability of which can be severely impaired under multicollinearity, CA explicitly reveals and quantifies existing interdependencies among variables. The difference is that effect sizes revealed by CA must be interpreted as the proportion of explained variance, whereas effect size in multiple linear regression is usually provided as slope coefficient representing the tightness of a relationship. Here, CA was used to account for multicollinearity to conceptualize unique and common effects of the remaining independent variables on ΔSOS_{GPP} and ΔEOS_{GPP}.

Pairwise correlations were therefore used as a pre-selection method to constrain the number of independent variables in CA, as the number of effects to interpret is exponentially proportional to the number of independent variables (i.e., a set of x variables results in $2^x - 1$ effects). A unique effect of a given independent variable was interpreted as a direct effect exerted independently from other variables (no mediation). Common effects represented by the variance shared by at least two independent variables were interpreted as indirect, or mediation effects. The effect of an environmental variable on ΔSOS_{GPP} and ΔEOS_{GPP} can be transmitted through a third variable; it is hence crucial to include possible mediation effects in the statistical framework. The sum of all unique and common effects of independent variable was interpreted

as the explanatory power of the CA model and corresponds with the coefficient of determination (R^2).

Next, unique and common effects that contributed to at least ±5 % of the total explained variation in ΔSOS_{GPP} (ΔEOS_{GPP}) were selected to construct the path diagrams for structural equation modeling (SEM; Wright, 1921; Jöreskog, 1970; Wold, 1975). Variables assigned as unique effects by the CA were incorporated as direct effects, whereas variables assigned as common effects were incorporated as indirect (mediation) effects. If an initial model, as hypothesized by the CA, was a poor fit of the data and not all paths were significant, new models were tested by iteratively removing the variable with the lowest non-significant standardized path coefficient, until all paths were significant, and the model was a good fit to the data. The Akaike information criterion (AIC; Akaike, 1973) was used to choose the most parsimonious model. As a last step, SEM was used as a confirmative approach to evaluate the constructed path diagrams (model selection criteria: p-value of the χ^2 statistic of a model is greater or equal than 0.05 and all paths are significant with a p-value less than 0.05). Statistical measures such as the χ^2 statistic are commonly used with SEM to assess the goodness-of-fit of a model, whereas R^2 are used in linear regression models. All analyses were conducted in MATLAB 2020a (MATLAB, 2020) and R (R Core Team, 2020) with the *yhat* and *lavaan* packages (Nimon *et al.*, 2008; Rosseel, 2012).

3. Results

The start- and end-of-season delineated with GPP varied between early April (DOY 98) and mid-May (DOY 134), and between mid-September (DOY 259) and late October (DOY 300; Table 3), respectively. The length-of-season delineated with GPP varied between 135 and 197 days, with

239 generally longer seasons in southern, permafrost-free forest stands (CA-Qfo and CA-Obs) and
240 shorter seasons in northern forests stands with permafrost (CA-SCC, US-Uaf and US-Prr; Table
241 3).

AmeriFlux-ID	Mean SOS_{GPP} (DOY)	Mean EOS_{GPP} (DOY)	Mean LOS_{GPP} (days)
CA-Qfo	117 (112;125)	291 (282;296)	174 (171;178)
CA-Obs	109 (98;122)	291 (283;300)	182 (164;197)
CA-SCC	122 (115;126)	267 (261;272)	145 (137;154)
US-Uaf	118 (111;134)	272 (264;285)	154 (135;166)
US-Prr	110 (102;118)	266 (259;274)	156 (153;172)

Table 3: Mean start-of-season (SOS_{GPP}), end-of-season (EOS_{GPP}), and length-of-season (LOS_{GPP}) delineated from daily gross primary productivity (GPP) at each study site. The minimum and maximum SOS_{GPP}, EOS_{GPP} and LOS_{GPP} are shown in parentheses. DOY: day-of-year.

242 US-Uaf and CA-Obs had the longest observation records for forest stands in the permafrost
243 zone and below the southern limit of permafrost, respectively (Figure 3). Not surprisingly, the
244 correlations obtained for these sites were indicative for the correlations obtained for the
245 aggregated sites with (Perm) and without permafrost (Perm-free). Pairwise correlation
246 coefficients indicated that ΔSOS_{Ta}, ΔSOS_{Ts}, ΔSOS_{PPI} and ΔSOS_{Snow} had significant correlations
247 with ΔSOS_{GPP} only in sites without permafrost (Figure 3a). In fall, ΔEOS_{Ts}, ΔEOS_{Snow},
248 $\Delta\overline{SWC_{JASO}}$ had significant correlations with ΔEOS_{GPP} in both, sites with and without permafrost
249 (Figure 3b).

250 Commonality analysis was used with ΔSOS_{Ta}, ΔSOS_{Ts} and ΔSOS_{PPI} as explanatory variables
251 to explain the variation in ΔSOS_{GPP}. ΔSOS_{Snow} was excluded from further analyses because the
252 complete disappearance of snow on the ground occurred after SOS_{GPP} and thus could not explain
253 the variation in SOS_{GPP} (Supplement S3). In agreement with findings of a previous study

254 (Pulliainen *et al.*, 2017), SOS_{Snow} occurred on average 8 and 9 days after SOS_{GPP} at sites with and
255 without permafrost, respectively. Similarly, SOS_{PPI} also tended to occur after SOS_{GPP}, yet
256 vegetation canopy development and biochemistry are changing continuously (Supplement S3).
257 In contrast, SOS_{Snow} is a binary indicator of snow presence or absence, thus we decided to keep

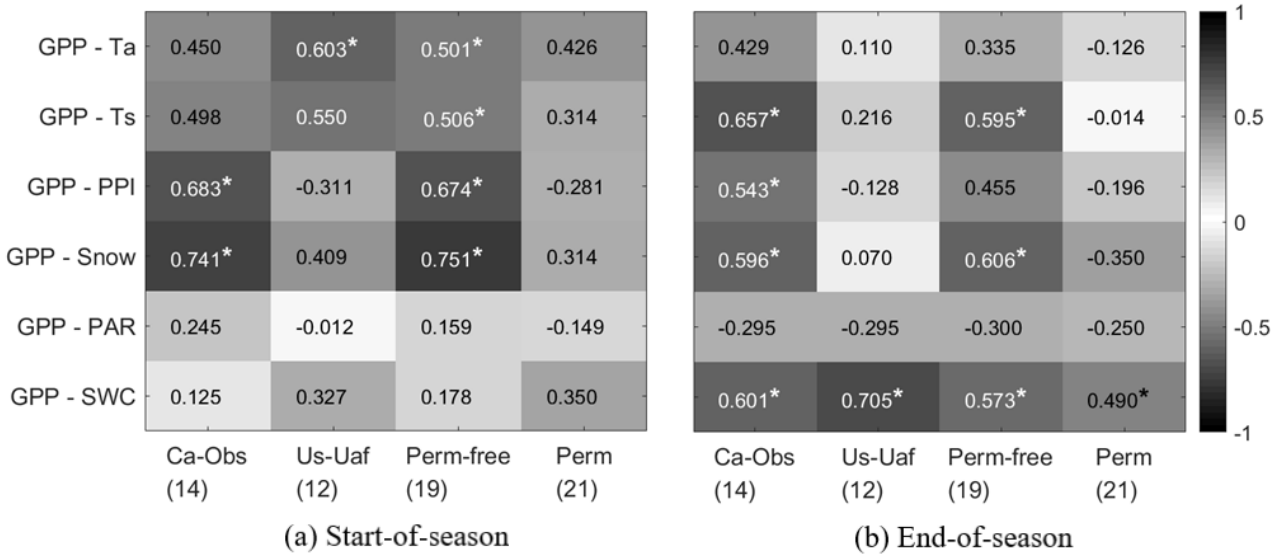

258 ΔSOS_{PPI} in further analyses but not SOS_{Snow}.

Figure 3: Correlation plots between the anomalies of (a) the start-of-season and (b) the end-of-season delineated from gross primary productivity (GPP) and environmental variables (Ta: air temperature; Ts: soil temperature; PPI: plant phenology index; Snow: snow-free period; PAR: photosynthetically active radiation; SWC: soil water content). Asterisks (*) indicate significant correlations ($\alpha = 0.05$). Results for individual sites are for US-Uaf and CA-Obs, as these sites had the highest number of years of observations from sites with (Perm) and without permafrost (Perm-free), respectively. The numbers of site-years are in parentheses.

259 For permafrost-free sites, around 74 % of the variance (R^2_{total}) in ΔSOS_{GPP} was explained
260 through the combination of ΔSOS_{Ta}, ΔSOS_{Ts} and ΔSOS_{PPI} (Table 4). The contribution of each of

the effects is relative to the total explained variance (i.e., variation explained by effects sums to 100 %). Unique effects on ΔSOS_{GPP} stemmed from ΔSOS_{Ts} and ΔSOS_{PPI}, whereas the unique effect of ΔSOS_{Ta} was negligible. All combinations of the environmental variables, including ΔSOS_{Ta}, had an impact on ΔSOS_{GPP} through common effects. These common effects were either joint temperature effects (ΔSOS_{Ta}, ΔSOS_{Ts}) or temperature effects mediated by canopy 'greenness' (ΔSOS_{PPI}). For sites with permafrost, ΔSOS_{Ta}, ΔSOS_{Ts} and ΔSOS_{PPI} explained only around 19 % of the variance in ΔSOS_{GPP} (Table 4). Unique effects on ΔSOS_{GPP} stemmed from ΔSOS_{Ta} and ΔSOS_{PPI}, and ΔSOS_{Ts} had no unique effect. Common effects of all environmental variables had a total effect size of around 66 %, with the largest proportion of variance covered by a Ts-mediated Ta effect.

Effect type	Interpretation	Contribution in % to R^2_{total} (R^2_{total} = 73.5 %): permafrost-free sites	Contribution in % to R^2_{total} (R^2_{total} = 19.2 %): sites with permafrost
ΔSOS_{Ta}	Unique air temperature effect	0.9	28.6*
ΔSOS_{Ts}	Unique soil temperature effect	21.1*	0.0
ΔSOS_{PPI}	Unique canopy 'greenness' effect	54.9*	5.7*
ΔSOS_{Ta} and ΔSOS_{Ts}	Soil temperature-mediated air temperature effect	16.2*	30.2*
ΔSOS_{Ta} and ΔSOS_{PPI}	Canopy 'greenness'-mediated air temperature effect	9.4*	14.5*
ΔSOS_{Ts} and ΔSOS_{PPI}	Canopy 'greenness'-mediated soil temperature effect	-10.1*	0.0
ΔSOS_{Ta}, ΔSOS_{Ts} and ΔSOS_{PPI}	Canopy 'greenness'-mediated temperature effect	7.6*	21.0*
Total		100.0	100.0

Table 4: Contribution of the explanatory variables to the total explained variance (R^2_{total}) in the anomalies (Δ) of the start-of-season delineated from daily gross primary productivity (ΔSOS_{GPP}).

Asterisks (*) indicate that the contribution to R^2_{total} is large enough (> ±5 %) to be integrated in the path analysis. SOS: start-of-season; Ta: air temperature; Ts: soil temperature; PPI: plant phenology index.

For ΔEOS_{GPP}, CA was used with ΔEOS_{Ts}, ΔEOS_{Snow} and $\Delta\overline{SWC_{JASO}}$ as explanatory variables. For permafrost-free sites, the combination of these variables explained around 57 % of the variation in ΔEOS_{GPP} (Table 5). Unique effects on ΔEOS_{GPP} stemmed from ΔEOS_{Snow} and $\Delta\overline{SWC_{JASO}}$. The largest proportion of the explained variance of ΔEOS_{GPP} was attributed to common effects (Table 5), particularly to a Ts-mediated SWC- and 'snow appearance' effect (i.e., the formation of a continuous snowpack). The same set of independent variables explained around 45 % of the variation in ΔEOS_{GPP} for sites with permafrost (Table 5). Only ΔEOS_{Snow} and $\Delta\overline{SWC_{JASO}}$ had a unique effect. The largest proportion of the variation was explained by the unique effect of $\Delta\overline{SWC_{JASO}}$. Only ΔEOS_{Snow} and $\Delta\overline{SWC_{JASO}}$ had a common effect, its negative contribution to R^2_{total} indicating a possible suppression effect (Horst, 1966; Seibold and McPhee, 1979).

Effect type	Interpretation	Contribution in % to R^2_{total} (R^2_{total} = 57.3%): permafrost-free sites	Contribution in % to R^2_{total} (R^2_{total} = 44.7%): sites with permafrost
ΔEOS_{Snow}	Unique snow appearance effect	23.0*	45.3*
ΔEOS_{Ts}	Unique soil temperature effect	2.7	3.5
$\Delta\overline{SWC_{JASO}}$	Unique soil moisture effect	17.2*	72.1*
ΔEOS_{Snow} and ΔEOS_{Ts}	Soil temperature-mediated snow appearance effect	17.0*	-2.5
ΔEOS_{Snow} and $\Delta\overline{SWC_{JASO}}$	Soil moisture-mediated snow appearance effect	-1.9	-17.4*

ΔEOS_{Ts} and $\Delta\overline{SWC_{JASO}}$	Soil temperature-mediated soil moisture effect	16.1*	-2.9
ΔEOS_{Snow}, ΔEOS_{Ts} and $\Delta\overline{SWC_{JASO}}$	Soil temperature-mediated soil moisture and snow appearance effect	25.9*	1.9
Total		100.0	100.0

Table 5: Contribution of the explanatory variables to the total explained variation (R^2_{total}) in the anomalies (Δ) of the end-of-season delineated from daily gross primary productivity (ΔEOS_{GPP}). Asterisks (*) indicate that the contribution to R^2_{total} is large enough (>±5 %) to be integrated in the path analysis. EOS: end-of-season; Ta: air temperature; Ts: soil temperature; SWC: soil water content; Snow: snow-free period; JASO: July-August-September-October.

Based on the CA, we constructed path diagrams to be tested with SEM, keeping the effects contributing to at least ±5 % of the total explained variation (Tables 4 and 5, Figures 4a and 5a). Unique effects were defined as direct effects, while common effects were accounted for as indirect effects, corresponding to mediation effects, in the path diagrams. The hypothesized path diagrams were the initial models to fit the data in spring (Figure 4a). Both path diagrams shared similar paths, except for the direct effect of ΔSOS_{Ta} on ΔSOS_{GPP} (gray arrow in Figure 4a), present at sites with permafrost but not at permafrost-free sites. These initial models were poor fits of the data (p-values of the paths > 0.05; not shown here).

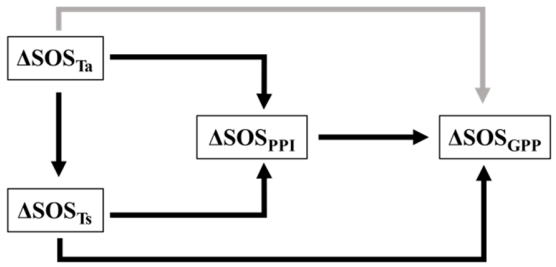

(a) Initial models (permafrost and permafrost-free)

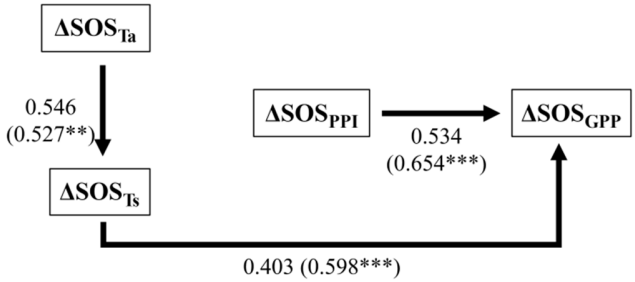

(b) Final model (permafrost-free)

Figure 4: (a) Hypothesized path diagrams tested with structural equation modeling for anomalies (Δ) in the start-of-season (SOS) delineated from gross primary productivity (ΔSOS_{GPP}), constructed with environmental variables selected with the commonality analysis. Black arrows indicate paths valid for both, sites with and without permafrost; the gray arrow indicates a path only valid for sites with permafrost. (b) Resulting path diagrams for ΔSOS_{GPP}. Black arrows indicate paths valid for permafrost-free sites only, as no model shows significant paths for sites with permafrost. Unstandardized path coefficients are shown alongside standardized coefficients in parentheses. Asterisks (*) indicate the p-value (* < 0.05, ** < 0.01, *** < 0.001). The χ^2 chi-square statistic, which assesses the goodness-of-fit, is 1.07 with a p-value of 0.584 on 2 degrees of freedom. Akaike information criterion of the final model is 16.7, compared to 23.2 for the initial model (a). The environmental variables are anomalies (Δ) of SOS: Ta: air temperature; Ts: soil temperature; PPI: plant phenology index.

After removing all non-significant paths, the final model at permafrost-free sites indicated that ΔSOS_{PPI} had a direct effect on ΔSOS_{GPP} (Figure 4b). Similarly, ΔSOS_{Ts} had a direct effect on ΔSOS_{GPP} and in addition acted as a mediator of ΔSOS_{Ta}. Thus, ΔSOS_{GPP} at permafrost-free sites was determined by ΔSOS_{PPI}, and by the time when Ta rose above freezing and thereby caused soil thaw (Ts > 0°C). As expected by the pairwise correlation coefficients and the CA (Figure 3a, Table 4), no model showed significant paths for sites with permafrost.

296

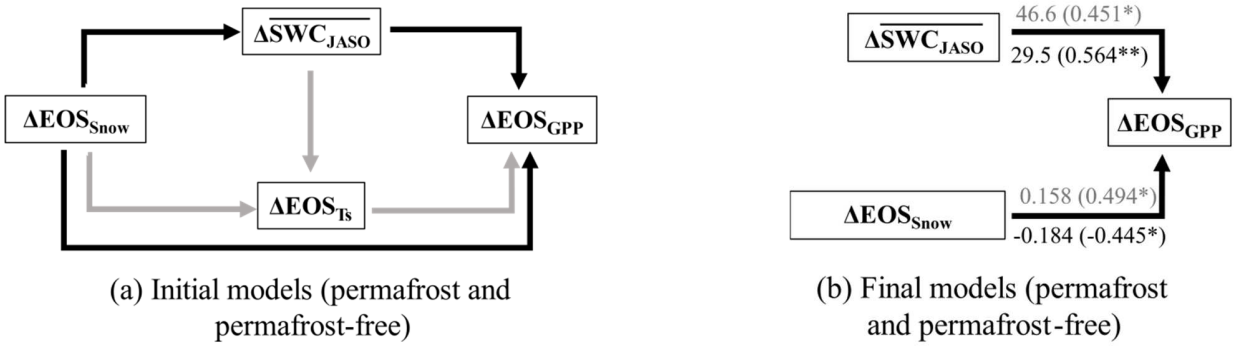

297

Figure 5: (a) Hypothesized path diagrams tested with structural equation modeling for anomalies (Δ) in the end-of-season (EOS) delineated from gross primary productivity (ΔEOS_{GPP}), constructed with environmental variables selected with the commonality analysis. Black arrows indicate paths valid for both, sites with and without permafrost; the gray arrows indicate paths only valid for permafrost-free sites. (b) Resulting path diagrams for ΔEOS_{GPP}. Black and gray path coefficients are for sites with and without permafrost, respectively. Unstandardized path coefficients are shown alongside standardized coefficients in parentheses. Stars indicate the p-value (* < 0.05, ** < 0.01, *** < 0.001). Final models for the sites with and without permafrost have an R^2 of 0.43 and 0.56 and an R^2_{adj} of 0.37 and 0.50, respectively. Akaike information criterion is 8.0 for both final models, compared to 14.0 and 24.0 for the initial models for the sites with and without permafrost (a). The environmental variables are the anomalies (Δ) of the end of the snow-free period (EOS_{Snow}) and of the late season (July-August-September-October; JASO) soil water content ($\overline{SWC_{JASO}}$).

298

299 For ΔEOS_{GPP}, the initial models for both, sites with and without permafrost, shared similar
300 paths with the difference that ΔEOS_{Ts} had an indirect effect on ΔEOS_{GPP} through ΔEOS_{Snow} and

301 $\Delta\overline{SWC_{JASO}}$ for permafrost-free sites only (Figure 5a). The final models indicated that the direct
302 effects of ΔEOS_{Snow} and $\Delta\overline{SWC_{JASO}}$ were the only significant paths on ΔEOS_{GPP} (Figure 5b). The
303 strength of the paths for $\Delta\overline{SWC_{JASO}}$ was similar for both categories of sites (with and without
304 permafrost). However, ΔEOS_{Snow} had contrasting effects on ΔEOS_{GPP} in sites with and without
305 permafrost, i.e., it is negative and positive, respectively.
306
307 **4. Discussion and conclusion**
308 This study sheds light on the explanatory power of different environmental variables known to
309 control growing season timing in black spruce-dominated boreal forest with and without
310 permafrost: canopy 'green-up' (ΔSOS_{PPI}), and air (ΔSOS_{Ta}) and soil temperature (ΔSOS_{Ts}) in
311 spring (ΔSOS_{GPP}), and soil water content ($\Delta\overline{SWC_{JASO}}$) and the formation of a continuous
312 snowpack (ΔEOS_{Snow}) in fall (ΔEOS_{GPP}).
313
314 **4.1 What controls the start of the growing season?**
315 The variation in ΔSOS_{GPP} at the permafrost-free sites was mostly explained by ΔSOS_{Ta} and
316 ΔSOS_{Ts}. As found in earlier studies (e.g., Suni *et al.*, 2003b; Barr *et al.*, 2009), SOS_{Ta} partly
317 explained SOS_{GPP}, and this study suggests that its control was mostly indirect via SOS_{Ts}. Above-
318 freezing Ta is necessary for the recovery of the reactions within photosystem II (Ensminger *et*
319 *al.*, 2004). In contrast to previous studies (e.g., Suni *et al.*, 2003b), we show that photosynthetic
320 recovery in spring also required unfrozen soil (Barr *et al.*, 2009). Earlier SOS_{Ta} resulted in earlier
321 thaw of near-surface soil layers, providing roots with access to liquid water. In a recent study at
322 CA-Obs, Pierrat *et al.* (2021) reported that above-freezing Ta and thawed stems were insufficient
323 for photosynthetic recovery of black spruce in spring. The difference in the timing between stem

rehydration and the onset of transpiration highlights the importance of access to liquid water in the soil for photosynthetic recovery in coniferous evergreen tree species. Viewed from the perspective of simple light use efficiency models (Monteith, 1972; 1977; Hilker et al., 2008) widely used in remote sensing communities (Ryu et al., 2019), low temperatures (Ta, Ts) resulting in limited access to liquid water may hamper photosynthetic recovery in spring by downregulating boreal forest stands' efficiency to relate absorbed PAR to photosynthetic CO_2 uptake, with potentially cascading effects on ΔSOS_{GPP}. In light use efficiency models, these effects might be enhanced or at least partially compensated for by PAR which is strongly influenced by variations in meteorological conditions.

The start of canopy 'green-up', ΔSOS_{PPI}, was significantly correlated with ΔSOS_{GPP} at the permafrost-free sites (Figure 3a). The remotely-sensed estimates of SOS_{PPI} occurred after SOS_{GPP} (Supplement S3). However, spectral vegetation indices such as PPI track continuously changing vegetation canopy development and associated changes in biochemistry functionally related to photosynthetic CO_2 uptake and thus its recovery in spring. Continuously changing vegetation canopy development and biochemistry are partly temperature-driven, but our results suggest that Ta and Ts appeared not to have had an indirect effect on ΔSOS_{GPP} through ΔSOS_{PPI}.

The start of the snow-free period, ΔSOS_{Snow}, was significantly correlated with ΔSOS_{GPP} at the permafrost-free sites (Figure 3a). A similarly strong correlation between SOS_{Snow} and SOS_{GPP} was reported for different boreal forest stands in the northern hemisphere (Pulliainen *et al.*, 2017). As SOS_{PPI}, the start of the snow-free period occurred after SOS_{GPP} (Supplement S3). Thus ΔSOS_{Snow} by itself was not a plausible explanation for ΔSOS_{GPP}. However, SOS_{Snow} may serve as proxy for photosynthetic recovery in spring since it is functionally related to SOS_{Ta} and SOS_{Ts}.

Soil water content, $\Delta\overline{SWC_{MAM}}$, and radiation, $\Delta\overline{PAR_{MAM}}$, posed no limits on photosynthetic

347 recovery for sites with or without permafrost (Figure 3a). Because of snowmelt, the amount of
348 available liquid water was not a limiting factor in spring (Iwata *et al.*, 2012; Arneth *et al.*, 2006).
349 Photoperiod increases rapidly in early spring, providing ample sunlight and thus PAR to
350 stimulate the reactions within the photosystem II. However, Ta is usually too low to activate the
351 chemical reactions in the Calvin cycle (Strand and Öquist, 1985), prohibiting photosynthetic
352 recovery in early spring despite sufficient PAR (Ensminger *et al.*, 2004).
353 No environmental variable, or combination of variables, significantly explained ΔSOS_{GPP} at
354 sites with permafrost, except for ΔSOS_{Ta} at US-Uaf (Figure 3a). We expected trees in forest
355 stands with permafrost to have more resource conservative life history strategies than their
356 counterparts below the southern limit of permafrost given the harsh environmental gradient
357 (Sniderhan *et al.*, 2018; Reich, 2014). Consequently, the ecophysiological functions of trees in
358 the permafrost zone might be less responsive to variation in environmental conditions and are
359 instead predominantly controlled by photoperiod (Sniderhan *et al.*, 2018; Reich, 2014). In
360 addition, differences in structure between forest stands with and without permafrost may partly
361 contribute to the differences in how environmental variables explained ΔSOS_{GPP}. Forest stands
362 with permafrost are characterized by relatively open canopies with low leaf area index (Table 1).
363 There, understory and ground cover vegetation make large contributions to ecosystem-level
364 water and carbon fluxes (e.g., Ikawa *et al.*, 2015). At US-Prr, trees contribute approximately 40
365 % to ecosystem-level water and carbon fluxes (Ikawa *et al.*, 2015). In contrast, at CA-Obs and
366 CA-Qfo, two forest stands without permafrost, trees contribute ca. 85 % to GPP (Gaumont-Guay
367 *et al.*, 2009; but also see Pappas *et al.*, 2020). In addition, the photosynthetic recovery of
368 coniferous evergreen tree species and evergreen understory vegetation may occur while the
369 ground is still covered by snow (e.g., Starr and Oberbauer, 2003). Deciduous broadleaf shrub
370 species comprising understory vegetation tend to produce leaves later in the season after

371 snowmelt is completed (Oberbauer *et al.*, 1998). Considering the important contributions of
372 understory and ground cover vegetation to ecosystem-level carbon and water fluxes, such
373 asynchronous seasonal trajectories in above- and belowground processes (Liu *et al.*, 2022) add
374 additional complexity when attempting to disentangle how environmental variables control
375 SOS_{GPP} in forest stands with permafrost.
376
377 **4.2 What controls the end of the growing season?**
378 Fewer studies have focused on how environmental variables control EOS_{GPP} (e.g., Liu *et al.*,
379 2022). Our results suggest that the variation in ΔEOS_{GPP} at both, sites with and without
380 permafrost, was explained by $\Delta\overline{SWC_{JASO}}$ and ΔEOS_{Snow}. Regardless of permafrost presence or
381 absence, SWC ($\Delta\overline{SWC_{JASO}}$) set a limit to the continuation of photosynthesis in fall, thus affecting
382 EOS_{GPP}. Soil water content in spring was higher and much less variable than in fall due to input
383 of liquid water through snowmelt. In contrast, SWC in fall largely depended on precipitation
384 inputs throughout the growing season. In addition, SWC in sites with permafrost also depended
385 on the depth of the seasonally thawed and hydrologically active layer above the frost table
386 (Quinton and Baltzer 2013). The permafrost-free sites were characterized by higher annual
387 precipitation compared to sites with permafrost (Table 1). The presence of impermeable
388 permafrost influences drainage since it restricts the movement of water to the active layer
389 (Quinton et al., 2019). Precipitation and drainage both affect SWC, which can be a limiting
390 factor for photosynthesis in the late season in boreal forests (Ruiz-Pérez and Vico, 2020). A
391 liquid water constraint in late growing season may therefore accelerate cessation of
392 photosynthesis by inducing stomatal closure to limit evaporative water loss to the atmosphere
393 (Reich *et al.*, 2018).

A complex finding of this study was the contrasting effect of ΔEOS_{Snow} on ΔEOS_{GPP} which was negative ($r = -0.45$, $p > 0.05$) in sites with permafrost and positive ($r = 0.41$, $p > 0.05$) in permafrost-free sites. It was not the timing of the formation of a continuous snowpack as such that influenced the end of photosynthesis, but rather the underlying meteorological conditions. At permafrost-free sites, formation of a continuous snowpack occurred later than for sites in the permafrost zone, causing precipitation to fall as rain rather than snow longer in fall (Lawrence and Slater, 2010). In contrast, formation of a continuous snowpack at sites with permafrost might occur later than at permafrost-free sites due to generally less precipitation at sites with permafrost. A later formation of a continuous snowpack implies a less insulated ground surface influenced by cold air, resulting in colder soils and thus an earlier cessation of photosynthesis in fall (Lawrence and Slater, 2010).

4.3 Limitations of the study

This study distinguished between boreal forest stands with and without permafrost. The total number of site-years ($n = 40$) was limited by data availability. The number of years of observations available per site differed, and the two categories of permafrost presence and absence were dominated by data from two sites, US-Uaf ($n = 12$) and CA-Obs ($n = 14$), respectively. Thus, results obtained for aggregated forest stands with ($n = 21$) and without permafrost ($n = 19$) largely reflect US-Uaf and CA-Obs, respectively (Figure 3). Undoubtedly, a larger dataset with more site-years containing all the studied environmental variables would be useful to better evaluate the generality of the findings we describe here. The number of boreal forest research sites where eddy covariance and supporting measurements are collected is growing (e.g., Helbig et al., 2020), however, the relatively small sample size ($n = 40$) highlights the importance and continued need for coordinated flux data collection efforts through network

418 initiatives such as FLUXNET, the National Ecological Observatory Network, or the Integrated
419 Carbon Observation System.
420 The methods and metrics used to delineate the start-of-season and end-of-season each have
421 their uncertainties, strengths, and limitations. For example, multiple methods to delineate SOS_{GPP}
422 and EOS_{GPP} and the start of canopy 'green-up' and end of canopy 'green-down' using spectral
423 vegetation indices (e.g., SOS_{PPI} and EOS_{PPI}) have been proposed (e.g., Karkauskaite *et al.*, 2017;
424 Kim *et al.*, 2012; Richardson *et al.*, 2010; Wang *et al.*, 2017). However, no single method was
425 suitable for the multi-site analyses of this study using diverse *in situ* (e.g., eddy covariance) and
426 remote sensing data streams (e.g., MODIS data product). In addition to the curve-fitting method
427 (Gonsamo *et al.*, 2013), a relative threshold method was tested to determine SOS_{GPP} and EOS_{GPP},
428 defined as the first and last DOY when daily GPP reaches a certain percentage of the annual
429 total, respectively (Barr *et al.*, 2009). In most years, the curve-fitting and threshold methods
430 provided comparable results. However, in years when a brief warm spell in early spring only
431 temporarily initiated photosynthetic recovery (e.g., in early April 2001 around DOY 100; Figure
432 2a), the curve fitting- and threshold-based estimates of SOS_{GPP} diverged (Supplement S4). Based
433 on visual inspection, the curve fitting-based estimates of SOS_{GPP} and EOS_{GPP} appeared to be the
434 most representative and plausible estimates across sites.
435 Although black spruce was the dominant tree species in all forest stands included in this
436 study, some scattered larch (*Larix laricina*) trees, a coniferous deciduous tree species, were also
437 present at CA-Qfo, CA-Obs and CA-SCC. Larch needles must emerge to initiate photosynthesis
438 in spring; hence their photosynthetic recovery occurred later than that of black spruce (Pierrat et
439 al., 2021). In addition, deciduous and evergreen understory and ground cover vegetation
440 occurred in all forest stands. The resulting diversity and structural complexity, and thus
441 asynchronicity in flux contributions across forest stands and footprints, was not resolved in

442 measurements of NEE made with eddy covariance techniques. The integrative nature of these
443 measurements challenged the delineation of SOS_{GPP} and EOS_{GPP}. Describing canopy 'greenness'
444 with spectral vegetation indices such as PPI using the MODIS MCD43A4 satellite product at
445 500-m spatial resolution faced similar challenges. Considering that boreal forests are interspersed
446 with lakes and wetlands, remotely-sensed estimates of SOS_{PPI} and EOS_{PPI} were representative of
447 fragmented landscapes characteristic for the boreal biome.
448 Daily gross primary productivity time series used in this study were derived from NEE
449 measured using eddy covariance techniques at five boreal forest sites. The gap-filling and
450 partitioning methods slightly differed across the sites. To evaluate the importance of such
451 methodological differences, a single gap-filling and partitioning method was also employed
452 across sites (Supplement S5). We used the REddyProcWeb online tool (Wutzler *et al.*, 2018)
453 based on Reichstein *et al.* (2005). The use of the consistent gap-filling and partitioning method
454 across sites resulted in unrealistic photosynthetic CO_2 uptake when air temperature was well
455 below freezing (e.g., DOY 0-10 in Figure S5.1a, DOY 40-50 in Figure S5.1b, DOY 325 in
456 Figure S5.1c and DOY 0-75 and DOY 325-350 in Figure S5.1d). Based on visual inspection we
457 decided to use daily GPP time series selected by site investigators as these were generally less
458 affected by such unrealistic photosynthetic CO_2 uptake in shoulder seasons.
459
460 **4.4 Implications**
461 Distinguishing between forest stands with and without permafrost, this study highlights how
462 environmental variables controlled the growing season timing of five boreal forest stands in
463 North America. The difference in how growing season timing was directly or indirectly
464 influenced (i.e., through 'mediation effects') by environmental variables was the most
465 pronounced in spring. However, understanding differences in mechanistic details of how

environmental variables control instantaneous and slow responses of the photosynthesis and the involved light and carbon reactions, and respiration (Kolari *et al.*, 2014; Wohlfahrt and Gu, 2015) at forest stands with and without permafrost warrants further investigation.

Amplified climate warming in high latitudes continues to accelerate permafrost thaw across the circumpolar permafrost zone (Biskaborn *et al.*, 2019). Projected climate change for the boreal biome (e.g., Gauthier *et al.*, 2015) and an associated northward shift of the southern limit of permafrost distribution imply rapidly changing environmental conditions. Thus, changes in the photosynthetic response of the boreal biome are to be expected. Such changes in the photosynthetic response of boreal forests due to permafrost thaw might range from changes in how environmental variables control photosynthesis and growing season timing as shown in this study, to a complete change in ecosystem composition and structure (e.g., loss of boreal forest and associated wetland expansion, Helbig *et al.*, 2016).

The representation of permafrost dynamics in land models used in Earth system models is receiving increased attention (e.g., Melton *et al.*, 2019). At the same time, land models have limited skill in reproducing above-ground vegetation phenology (Richardson *et al.*, 2011; Seiler *et al.*, 2022), and below-ground phenology poses an even greater challenge for such models (Liu *et al.*, 2022). A better understanding of how environmental controls of growing season timing in boreal forests are influenced by the presence or absence of permafrost is important for refined parameterizations of the boreal biome in Earth system models.

Acknowledgments

This study was supported in part by the Fonds de Recherche du Québec - Nature et Technologie (FRQNT) and CFREF Global Water Futures project Northern Water Futures. O.S. acknowledges funding by the Canada Research Chairs, Canada Foundation for Innovation Leaders Opportunity

Fund, and Natural Sciences and Engineering Research Council Discovery Grant programs. Funding for AmeriFlux data resources was provided by the U.S. Department of Energy's Office of Science. The CA-Obs site received support from Environment and Climate Change Canada, the Canadian Forest Service, the Fluxnet-Canada Research Network, the Canadian Carbon Program, the Cold Regions Research Network, and the Global Institute for Water Security. The US-Uaf and US-Prr sites were supported by the Arctic Challenge for Sustainability (ArCS; JPMXD1300000000) project, ArCS II (JPMXD1420318865). We also acknowledge the use of FLUXNET data, and the work of Hank Margolis and Carole Coursolle (Fluxnet-Canada Research Network/ Canadian Carbon Program). We thank Manuel Helbig, Joe Melton and the two anonymous reviewers for their constructive comments which substantially improved the quality of the manuscript.

Appendix A Plant phenology index

The plant phenology index (PPI; Jin and Eklundh, 2014) can be calculated using the MODIS MCD43A4 Nadir Bidirectional Reflectance Distribution Function-Adjusted Reflectance product with a 500-m resolution:

$$\mathrm{PPI} = -K \times \ln\frac{M - DVI}{M - DVI_S} \quad (1)$$

where DVI is the difference vegetation index, i.e., the difference between NIR and red reflectances, DVI_S is the DVI of the soil, which is empirically set to 0.09 (Karkauskaite *et al.*, 2017), and M is the maximum DVI. K is a gain factor given by:

$$K = \frac{0.25\ \cos(\theta)}{(1 - d_c)G + d_c \cos(\theta)} \cdot \frac{1 + M}{1 - M} \quad (2)$$

where θ is the solar zenith angle at local solar noon. G is a geometric function of leaf angular distribution (set to 0.5 after Karkauskaite *et al.*, 2017), and d_c is an instantaneous diffuse fraction of solar radiation for a given solar zenith angle. For clear-sky and standard atmosphere it is formulated as:

$$d_c = 0.0336 + \frac{0.0477}{\cos(\theta)} \quad (3)$$

References

Ahmed, H. F., Helgason, W., Barr, A., and Black, T. A. (2021). Characterization of spring thaw and its relationship with carbon uptake for different types of southern boreal forest. *Agric. For. Meteorol.*, 307:10851.

Akaike, H. (1973). Maximum likelihood identification of Gaussian autoregressive moving average models. *Biometrika*, 60(2):255–265.

Alwin, D. F., and Hauser, R. M. (1975). The decomposition of effects in path analysis. *Am. Sociol. Rev.*, 40(1):37–47.

Anderson, D. B. (1936). Relative humidity or vapor pressure deficit. *Ecology*, 17(2):277–282.

Arneth, A., Lloyd, J., Shibistova, O., Sogachev, A., and Kolle, O. (2006). Spring in the boreal environment: observations on pre-and post-melt energy and CO_2 fluxes in two central Siberian ecosystems. *Boreal Environ. Res.*, 11(4):311–328.

Badeck, F.-W., Bondeau, A., Bottcher, K., Doktor, D., Lucht, W., Schaber, J., and Sitch, S. (2004). Responses of spring phenology to climate change. *New Phytol.*, 162(2):295–309.

Baldocchi, D., and Meyers, T. (1998). On using eco-physiological, micrometeorological and biogeochemical theory to evaluate carbon dioxide, water vapor and trace gas fluxes over vegetation: a perspective. *Agric. For. Meteorol.*, 90(1-2):1–25.

Baron, R. M., and Kenny, D. A. (1986). The moderator–mediator variable distinction in social psychological research: Conceptual, strategic, and statistical considerations. *J. Pers. Soc. Psychol.*, 51(6):173-1182.

534 Barr, A. G., Black, T., Hogg, E., Kljun, N., Morgenstern, K., and Nesic, Z. (2004). Interannual
535 variability in the leaf area index of a boreal aspen-hazelnut forest in relation to net ecosystem
536 production. *Agric. For. Meteorol.*, 126(3-4):237–255.

537 Barr, A., Morgenstern, K., Black, T., McCaughey, J., and Nesic, Z. (2006). Surface energy
538 balance closure by the eddy-covariance method above three boreal forest stands and
539 implications for the measurement of the CO_2 flux. *Agric. For. Meteorol.*, 140(1-4):322–337.

540 Barr, A., Black, T. A., and McCaughey, H. (2009). Climatic and phenological controls of the
541 carbon and energy balances of three contrasting boreal forest ecosystems in western Canada.
542 In Noormets, A. (eds) *Phenology of Ecosystem Processes*, pp. 3–23. Springer, New York, NY.

543 Barr, A., van der Kamp, G., Black, T., McCaughey, J., and Nesic, Z. (2012). Energy balance
544 closure at the BERMS flux towers in relation to the water balance of the White Gull Creek
545 watershed 1999–2009. *Agric. For. Meteorol.*, 153:3–13.

546 Bergeron, O., Margolis, H. A., Black, T. A., Coursolle, C., Dunn, A. L., Barr, A. G., and Wofsy,
547 S. C. (2007). Comparison of carbon dioxide fluxes over three boreal black spruce forests in
548 Canada. *Glob. Chang. Biol.*, 13(1):89–107.

549 Biskaborn, B. K., Smith, S. L., Noetzli, J., Matthes, H., Vieira, G., Streletskiy, D. A., ... and
550 Lantuit, H. (2019). Permafrost is warming at a global scale. *Nat. Commun.*, 10:264.

551 Black, T. A., Gaumont-Guay, D., Jassal, R. S., Amiro, B., Jarvis, P. G., Gower, T., Kelliher, F.,
552 Dunn, A., and Wofsy, S. (2004). Measurement of CO_2 exchange between boreal forest and the
553 atmosphere. In Griffis, H. and Jarvis, P. G. (eds) *Carbon Balance of Forest Biomes*, pp. 120–
554 141. Taylor & Francis.

555 Bowling, D. R., Logan, B. A., Hufkens, K., Aubrecht, D. M., Richardson, A. D., Burns, S. P.,
556 Anderegg, W. R. L., Blanken, P. D., and Eiriksson, D. P. (2018). Limitations to winter and
557 spring photosynthesis of a Rocky Mountain subalpine forest. *Agric. For. Meteorol.*, 252:241-
558 255,

559 Brandt, J. (2009). The extent of the North American boreal zone. *Environmental Rev.*, 17:101–
560 161.

561 Brown, J., Ferrians, O., Heginbottom, J. A., and Melnikov, E. (2002). *Circum-Arctic Map of*
562 *Permafrost and Ground-Ice Conditions, Version 2.* NSIDC: National Snow and Ice Data
563 Center. Boulder, Colorado USA. Accessed August 13, 2020.

564 Brown, R. D., and Mote, P. W. (2009). The response of northern hemisphere snow cover to a
565 changing climate. *J. Clim.*, 22(8):2124–2145.

566 Buermann, W., Forkel, M., O'Sullivan, M., Sitch, S., Friedlingstein, P., Haverd, V., Jain, A. K.,
567 Kato, E., Kautz, M., Lienert, S., Lombardozzi, D., Nabel, J., Tian, H., Wiltshire, A., Zhu, D.,
568 Smith, W. K., and Richardson, A. D. (2018). Widespread seasonal compensation effects of
569 spring warming on northern plant productivity. *Nature*, 562**:**110–114.

570 Chen, J. M., Chen, B., Higuchi, K., Liu, J., Chan, D., Worthy, D., Tans, P., and Black, A. (2006).
571 Boreal ecosystems sequestered more carbon in warmer years. *Geophys. Res. Lett.*,
572 33(10):L10803.

573 Commission for Environmental Cooperation (2011). North America Political Boundary. United
574 States Geological Survey.
575 https://www.sciencebase.gov/catalog/item/4fb555ebe4b04cb937751db9. Accessed August 13,
576 2020.

577 Delpierre, N., Vitasse, Y., Chuine, I., Guillemot, J., Bazot, S., Rutishauser, T., and Rathgeber, C.
578 B. K. (2016). Temperate and boreal forest tree phenology: from organ-scale processes to
579 terrestrial ecosystem models. *Ann. For. Sci.*, 73(1):5–25.

580 Dunn, A. L., Barford, C. C., Wofsy, S. C., Goulden, M. L., and Daube, B. C. (2007). A longterm
581 record of carbon exchange in a boreal black spruce forest: means, responses to interannual
582 variability, and decadal trends. *Glob. Chang. Biol.*, 13(3):577–590.

583 Edwards, A. C., and Cresser, M. S. (1992). Freezing and its effect on chemical and biological
584 properties of soil. *Adv. Soil Sci.,* 18, 59-79.

585 Ensminger, I., Sveshnikov, D., Campbell, D. A., Funk, C., Jansson, S., Lloyd, J., Shibistova, O.,
586 and Öquist, G. (2004). Intermittent low temperatures constrain spring recovery of
587 photosynthesis in boreal Scots pine forests. *Glob. Chang. Biol.*, 10(6):995–1008.

588 Gaumont-Guay, D., Black, T. A., McCaughey, H., Barr, A. G., Krishnan, P., Jassal, R. S., and
589 Nesic, Z. (2009). Soil CO_2 efflux in contrasting boreal deciduous and coniferous stands and its
590 contribution to the ecosystem carbon balance. *Glob. Chang. Biol.*, 15(5):1302–1319.

591 Gauthier, S., Bernier, P., Kuuluvainen, T., Shvidenko, A. Z., and Schepaschenko, D. G. (2015).
592 Boreal forest health and global change. *Science*, 349(6250):819–822.

593 Gonsamo, A., Chen, J. M., and D'Odorico, P. (2013). Deriving land surface phenology indicators
594 from CO_2 eddy covariance measurements. *Ecol. Indic.*, 29:203–207.

595 Gruber, S. (2012). Derivation and analysis of a high-resolution estimate of global permafrost
596 zonation. *The Cryosphere*, 6(1):221–233.

597 Harris, S., French, H., Heginbottom, J., Johnston, G., Ladanyi, B., Sego, D., and van Everdingen,
598 R. (1988). Glossary of permafrost and related ground-ice terms. *Associate Committee on*
599 *Geotechnical Research, National Research Council of Canada*.

600 Helbig, M., Chasmer, L. E., Desai, A. R., Kljun, N., Quinton, W. L., and Sonnentag, O. (2017).
601 Direct and indirect climate change effects on carbon dioxide fluxes in a thawing boreal forest-
602 wetland landscape. *Glob. Chang. Biol.*, 23(8):3231–3248.

603 Helbig, M., Pappas, C., and Sonnentag, O. (2016). Permafrost thaw and wildfire: Equally
604 important drivers of boreal tree cover changes in the Taiga Plains, Canada. *Geophys. Res.*
605 *Lett.*, 43(4):1598–1606.

606 Helbig, M., Waddington, J. M., Alekseychik, P., Amiro, B. D., Aurela, M., Barr, A. G., ..., and
607 Zyrianov, V. (2020). Increasing contribution of peatlands to boreal evapotranspiration in a
608 warming climate. *Nat. Clim. Chang.*, 10(6):555-560.

609 Hilker, T., Coops, N. C., Wulder, M. A., Black, T. A., Guy, R. D. (2008). The use of remote
610 sensing in light use efficiency-based models of gross primary production: a review of current
611 status and future requirements. *Sci. Total Environ.*, 404: 411-423.

612 Horst, P. (1966). *Psychological Measurement and Prediction*. Wadsworth, Belmont, CA.

613 Ikawa, H., Nakai, T., Busey, R. C., Kim, Y., Kobayashi, H., Nagai, S., Ueyama, M., Saito, K.,
614 Nagano, H., Suzuki, R., and Hinzman, L. (2015). Understory CO_2, sensible heat, and latent
615 heat fluxes in a black spruce forest in interior Alaska. *Agric. For. Meteorol.*, 214:80–90.

616 Iwata, H., Harazono, Y., and Ueyama, M. (2012). The role of permafrost in water exchange of a
617 black spruce forest in Interior Alaska. *Agric. For. Meteorol.*, 161:107–115.

618 Jin, H., and Eklundh, L. (2014). A physically based vegetation index for improved monitoring of
619 plant phenology. *Remote Sens. Environ.*, 152:512–525.

620 Jin, H., Jönsson, A. M., Bolmgren, K., Langvall, O., and Eklundh, L. (2017). Disentangling
621 remotely-sensed plant phenology and snow seasonality at northern Europe using MODIS and
622 the plant phenology index. *Remote Sens. Environ.*, 198:203–212.

623 Jönsson, A. M., Eklundh, L., Hellström, M., Bärring, L., and Jönsson, P. (2010). Annual changes
624 in MODIS vegetation indices of Swedish coniferous forests in relation to snow dynamics and
625 tree phenology. *Remote Sens. Environ.*, 114(11):2719–2730.

626 Jöreskog, K. G. (1970). A general method for estimating a linear structural equation system. *ETS*
627 *Research Bulletin Series*, 1970(2):1–41.

628 Karkauskaite, P., Tagesson, T., and Fensholt, R. (2017). Evaluation of the plant phenology index
629 (PPI), NDVI and EVI for start-of-season trend analysis of the Northern Hemisphere boreal
630 zone. *Remote Sen.*, 9(5):485.

631 Kim, Y., Kimball, J., Zhang, K., and McDonald, K. (2012). Satellite detection of increasing
632 Northern Hemisphere non-frozen seasons from 1979 to 2008: Implications for regional
633 vegetation growth. *Remote Sens. Environ.*, 121:472–487.

634 Kobayashi, H., Yunus, A. P., Nagai, S., Sugiura, K., Kim, Y., Van Dam, B., Nagano, H., Zona,
635 D., Harazono, Y., Bret-Harte, M. S., Ichii, K., Ikawa, H., Iwata, H., Oechel, W. C., Ueyama,
636 M., and Suzuki, R. (2016). Latitudinal gradient of spruce forest understory and tundra
637 phenology in Alaska as observed from satellite and ground-based data. *Remote Sens. Environ.*,
638 177:160–170.

639 Koebsch, F., Sonnentag, O., Järveoja, J., Peltoniemi, M., Alekseychik, P., Aurela, M., Arslan, A.
640 N., Dinsmore, K., Gianelle, D., Helfter, C., Jackowicz-Korczynski, M., Korrensalo, A., Leith,
641 F., Linkosalmi, M., Lohila, A., Lund, M., Maddison, M., Mammarella, I., Mander, Ü.,
642 Minkkinnen, K., Pickard, A., Pullens, J. W. M., Tuittila, E.-S., Nilsson, M. B., and Peichl, M.
643 (2020). Refining the role of phenology in regulating gross ecosystem productivity across
644 European peatlands. *Glob. Chang. Biol.*, 26(2):876–887.

645 Kolari, P., Chan, T., Porcar-Castell, A., Baeck, J., Nikinmaa, E., and Juurola, E. (2014). Field
646 and controlled environment measurements show strong seasonal acclimation in
647 photosynthesis and respiration potential in boreal Scots pine. *Front. Plant. Sci.*, 5:717.

648 Krishnan, P., Black, T. A., Barr, A. G., Grant, N. J., Gaumont-Guay, D., and Nesic, Z. (2008).
649 Factors controlling the interannual variability in the carbon balance of a southern boreal black
650 spruce forest. *J. Geophys. Res. Atmos.*, 113:D09109.

651 Lawrence, D. M., and Slater, A. G. (2010). The contribution of snow condition trends to future
652 ground climate. *Clim. Dyn.*, 34(7-8):969–981

653 Liu, H., Wang, H., Li, N., Shao, J., Zhou, X., van Groenigen, K. J., and Thakur, M. P. (2022).
654 Phenological mismatches between above-and belowground plant responses to climate
655 warming. *Nat. Clim. Chang.*, 12(1):97-102.

656 Magney, T. S., Bowling, D. R., Logan, B. A., Grossmann, K., Stutz, J., Blanken, P. D., Burns, S.
657 P., Cheng, R., Garcia M. A., Köhler, P., Lopez, S., Parazoo, N. C., Raczka, B., Schimel, D.,
658 and Frankenberg, C. (2019). Mechanistic evidence for tracking the seasonality of
659 photosynthesis with solar-induced fluorescence. *Proc. Nat. Acad. Sci. U.S.A.*, 116(24):11640-
660 11645.

MATLAB (2020). 9.5.0.944444 (2020a). The MathWorks Inc. Matick, Massachusetts, USA.

Melton, J. R., Verseghy, D. L., Sospedra-Alfonso, R., and Gruber, S. (2019). Improving permafrost physics in the coupled Canadian Land Surface Scheme (v.3.6.2) and Canadian Terrestrial Ecosystem Model (v.2.1) (CLASS-CTEM). *Geosci. Model Dev.*, 12:4443-4467.

Mood, A. M. (1969). Macro-analysis of the American educational system. *Oper. Res.*, 17(5):770–784.

Monteith, J. L. (1972). Solar radiation and productivity in tropical ecosystems. *J. Appl. Ecol.*, 9: 747-766.

Monteith, J. L. (1977). Climate and efficiency of crop production in Britain. *Philos. Trans. R. Soc. Lond., B, Bio. Sci.* 281, 277–294.

Newton, R., and Spurrell, D. (1967). A development of multiple regression for the analysis of routine data. *J. R. Stat. Soc. Ser. C. App. Stat.*, 16(1):51–64.

Nilsson, S., Shvidenko, A., Stolbovoi, V., Gluck, M., Jonas, M., and Obersteiner, M. (2000). Full carbon account for Russia. *International Institute for Applied Systems Analysis Interim Report IR-00-021*.

Nimon, K., Lewis, M., Kane, R., and Haynes, R. M. (2008). An R package to compute commonality coefficients in the multiple regression case: An introduction to the package and a practical example. *Beh. Res. Methods*, 40(2):457–466.

Oberbauer, S. F., Starr, G., and Pop, E. W. (1998). Effects of extended growing season and soil warming on carbon dioxide and methane exchange of tussock tundra in Alaska. *J. Geophys. Res. Atmos.*, 103(D22):29075-29082.

682 ORNL DAAC (2018). MODIS and VIIRS land products global subsetting and visualization tool.
683 ORNL DAAC, Oak Ridge, Tennessee, USA. Accessed June 10, 2020. Subset obtained for
684 MCD43A4 product at various sites in Spatial Range: N=65.12, S=49.49, E=74.34W,
685 W=147.86W, time period: 2000 to 2020, and subset size: 0.5 x 0.5 km. doi:
686 10.3334/ORNLDAAC/1379.

687 Öquist, G., and Huner, N. P. (2003). Photosynthesis of overwintering evergreen plants. *Annu.*
688 *Rev. Plant Biol.*, 54(1):329-355.

689 Pappas, C., Maillet, J., Rakowski, S., Baltzer, J.L., Barr, A. G., Black, T. A., Fatichi, S.,
690 Laroque, C. P., Matheny, A. M., Roy, A., Sonnentag, O., and Zha, T. (2020). Aboveground
691 tree growth is a minor and decoupled fraction of boreal forest carbon input. *Agric. For.*
692 *Meteorol.*, 290:108030.

693 Parazoo, N. C., Arneth, A., Pugh, T. A., Smith, B., Steiner, N., Luus, K., Commane, R.,
694 Benmergui, J., Stofferahn, E., Liu, J., Rödenbeck, C., Kawa, R., Euskirchen, E., Zona, D.,
695 Arndt, K., Oechel, W., and Miller, C. (2018). Spring photosynthetic onset and net CO_2 uptake
696 in Alaska triggered by landscape thawing. *Glob. Chang. Biol.*, 24(8):3416–3435.

697 Piao, S., Ciais, P., Friedlingstein, P., Peylin, P., Reichstein, M., Luyssaert, S., Margolis, H.,
698 Fang, J., Barr, A., Chen, A., Grelle, A., Hollinger, D. Y., Laurila, T., Lindroth, A.,
699 Richardson, A. D., and Vesala, T. (2008). Net carbon dioxide losses of northern ecosystems in
700 response to autumn warming. *Nature*, 451(7174): 49-52.

701 Pierrat, Z., Nehemy, M. F., Roy, A., Magney, T., Parazoo, N. C., Laroque, C., Pappas, C.,
702 Sonnentag, O., Grossmann, K., Bowling, D. R., Seibt, U., Ramirez, A., Johnson, B.,
703 Helgason, W., Barr, A., and Stutz, J. (2021). Tower-based remote sensing reveals mechanisms

behind a two-phased spring transition in a mixed-species boreal forest. J. Geophys. Res. Biogeosci., 126(5):e2020JG006191.

Pulliainen, J., Aurela, M., Laurila, T., Aalto, T., Takala, M., Salminen, M., Kulmala, M., Barr, A., Heimann, M., Lindroth, A., Laaksonen, A., Derksen, C., Mäkelä, A., Markkanen, T., Lemmetyinen, J., Susiluoto, J., Dengel, S., Mammarella, I., Tuovinen, J.-P., and Vesala, T. (2017). Early snowmelt significantly enhances boreal springtime carbon uptake. *Proc. Nat. Acad. Sci. U.S.A.*, 114(42):11081–11086.

Quinton, W. L., and Baltzer, J. L. (2013). The active-layer hydrology of a peat plateau with thawing permafrost (Scotty Creek, Canada). *Hydrogeol. J.*, 21(1):201-220.

Quinton, W., Berg, A., Braverman, M., Carpino, O., Chasmer, L., Connon, R., Craig, J., Devoie, É., Hayashi, M., Haynes, K., Olefeldt, D., Pietroniro, A., Rezanezhad, F., Schincariol, R., and Sonnentag, O. (2019). A synthesis of three decades of hydrological research at Scotty Creek, NWT, Canada. *Hydrol. Earth Syst. Sci*., 23(4):2015-2039.

R Core Team (2020). R: A language and environment for statistical computing. R Foundation for Statistical Computing. Vienna, Austria.

Ray-Mukherjee, J., Nimon, K., Mukherjee, S., Morris, D. W., Slotow, R., and Hamer, M. (2014). Using commonality analysis in multiple regressions: a tool to decompose regression effects in the face of multicollinearity. *Methods Ecol. Evol.*, 5(4):320–328.

Reich, P. B. (2014). The world-wide 'fast-slow' plant economics spectrum: a traits manifesto. *J. Ecol.*, 102(2):275–301.

724 Reich, P. B., Sendall, K. M., Stefanski, A., Rich, R. L., Hobbie, S. E., and Montgomery, R. A.
725 (2018). Effects of climate warming on photosynthesis in boreal tree species depend on soil
726 moisture. *Nature*, 562(7726):263–267.

727 Reichstein, M., Falge, E., Baldocchi, D., Papale, D., Aubinet, M., Berbigier, P., Bernhofer, C.,
728 Buchmann, N., Gilmanov, T., Granier, A., Grünwald, T., Havránková, K., Ilvesniemi, H.,
729 Janous, D., Knohl, A., Laurila, T., Lohila, A., Loustau, D., Matteucci, G., Meyers, T.,
730 Miglietta, F., Ourcival, J.-M., Pumpanen, J., Rambal, S., Rotenberg, E., Sanz, M., Tenhunen,
731 J., Seufert, G., Vaccari, F., Vesala, T., Yakir, D., and Valentini, R. (2005). On the separation
732 of net ecosystem exchange into assimilation and ecosystem respiration: review and improved
733 algorithm. *Glob. Chang. Biol.*, 11(9):1424–1439.

734 Richardson, A. D., Black, T. A., Ciais, P., Delbart, N., Friedl, M. A., Gobron, N., Hollinger, D.
735 Y., Kutsch, W. L., Longdoz, B., Luyssaert, S., Migliavacca, M., Montagnani, L., William
736 Munger, J., Moors, E., Piao, S., Rebmann, C., Reichstein, M., Saigusa, N., Tomelleri, E.,
737 Vargas, R., and Varlagin, A. (2010). Influence of spring and autumn phenological transitions
738 on forest ecosystem productivity. *Philos. Trans. R. Soc. Lond., B, Bio. Sci.*, 365(1555):3227–
739 3246.

740 Richardson, A. D., Anderson, R. S., Arain, M. A., Barr, A. G., Bohrer, G., Chen, G., Chen, J. M.,
741 Ciais, P., Davis, K. J., Desai, A. R., Dietze, M. C., Dragoni, D., Garrity, S. R., Gough, C. M.,
742 Grant, R., Hollinger, D. Y., Margolis, H. A., McCaughey, H., Migliavacca, M., Monson, R.
743 K., Munger, J. W., Poulter, B., Raczka, B. M., Ricciuto, D. M., Sahoo, A. K., Schaefer, K.,
744 Tian, H., Vargas, R., Verbeeck, H., Xiao, J., and Xue, Y. (2011). Terrestrial biosphere models
745 need better representation of vegetation phenology: results from the North American Carbon
746 Program Site Synthesis. *Glob. Chang. Biol.*, 18(2):566-584.

747 Richardson, A. D., Keenan, T. F., Migliavacca, M., Ryu, Y., Sonnentag, O., and Toomey, M.
748 (2013). Climate change, phenology, and phenological control of vegetation feedbacks to the
749 climate system. *Agric. For. Meteorol.*, 169:156–173.

750 Rosseel, Y. (2012). lavaan: An R Package for Structural Equation Modeling. *J. Stat. Softw.*,
751 48(2) :1–36.

752 Roy, A., Toose, P., Mavrovic, A., Pappas, C., Royer, A., Derksen, C., Berg, A., Rowlandson, T.,
753 El- Amine, M., Barr, A., Black, T. A., Langlois, A., and Sonnentag, O. (2020). L-band
754 response to freeze/thaw in a boreal forest stand from ground-and tower-based radiometer
755 observations. *Remote Sens. Environ.*, 237:111542.

756 Runkle, B. R. K., Sachs, T., Wille, C., Pfeiffer, E.-M., and Kutzbach, L. (2013). Bulk
757 partitioning the growing season net ecosystem exchange of CO_2 in Siberian tundra reveals the
758 seasonality of its carbon sequestration strength. *Biogeosciences*, 10:1337–1349.

759 Ruiz-Pérez, G., and Vico, G. (2020). Effects of temperature and water availability on Northern
760 European boreal forests. *Front. For. Glob. Change*, 3:34.

761 Ryu, Y., Berry, J. A., Baldocchi, D. D. (2019). What is global photosynthesis? History,
762 uncertainties and opportunities. *Remote Sens. Environ.*, 223:95-114.

763 Schaaf, C., and Wang, Z. (2015). MCD43A4 MODIS/Terra+Aqua BRDF/Albedo Nadir BRDF
764 Adjusted RefDaily L3 Global - 500m V006. *NASA EOSDIS Land Processes DAAC*. doi:
765 10.5067/MODIS/MCD43A4.006.

766 Seibold, D. R., and McPhee, R. D. (1979). Commonality analysis: A method for decomposing
767 explained variance in multiple regression analyses. *Hum. Commun. Res.*, 5(4):355–365.

768 Seiler, C., Melton, J. R., Arora, V., Sitch, S., Friedlingstein, P., Arneth, A., Goll, D. S., Jain, A.,
769 Joetzjer, E., Lienert, S., Lombardozzi, D., Luyssaert, S., Nabel, J. E. M. S., Tian, H., Vuichard,
770 N., Walker, A. P., Yuan, W., and Zaehle, S. (2022). Are terrestrial biosphere models fit for
771 simulating the global land carbon sink? *J. Adv. Model. Earth Syst.*, e2021MS002946.

772 Shur, Y. L., and Jorgenson, M. T. (2007). Patterns of permafrost formation and degradation in
773 relation to climate and ecosystems. *Permafrost and Periglac. Process.*, 18(1):7-19.

774 Sniderhan, A. E., McNickle, G. G., and Baltzer, J. L. (2018). Assessing local adaptation vs.
775 plasticity under different resource conditions in seedlings of a dominant boreal tree species.
776 *AoB Plants*, 10(1):ply004.

777 Starr, G., and Oberbauer, S. F. (2003). Photosynthesis of arctic evergreens under snow:
778 implications for tundra ecosystem carbon balance. *Ecology*, 84(6):1415–1420.

779 Strand, M., and Öquist, G. (1985). Inhibition of photosynthesis by freezing temperatures and
780 high light levels in cold-acclimated seedlings of Scots pine (Pinus sylvestris).-I. effects on the
781 light-limited and light-saturated rates of CO_2 assimilation. *Physiol. Plant.* 64(4):425–430.

782 Suni, T., Berninger, F., Markkanen, T., Keronen, P., Rannik, U., and Vesala, T. (2003a).
783 Interannual variability and timing of growing-season CO_2 exchange in a boreal forest. *J.*
784 *Geophys. Research Atmos.*, 108(D9):4265–4272.

785 Suni, T., Berninger, F., Vesala, T., Markkanen, T., Hari, P., Makela, A., Ilvesniemi, H.,
786 Hanninen, H., Nikinmaa, E., Huttula, T., Laurila, T., Aurela, M., Grelle, A., Lindroth, A.,
787 Arneth, A., Shibistova, O., and Lloyd, J. (2003b). Air temperature triggers the recovery of
788 evergreen boreal forest photosynthesis in spring. *Glob. Chang. Biol.*, 9(10):1410–1426.

789 Tucker, C. J. (1979). Red and photographic infrared linear combinations for monitoring
790 vegetation. *Remote Sens. Environ.*, 8(2):127–150.

791 Ueyama, M., Iwata, H., and Harazono, Y. (2014). Autumn warming reduces the CO_2 sink of a
792 black spruce forest in interior Alaska based on a nine-year eddy covariance measurement.
793 *Glob. Chang. Biol.*, 20(4):1161–1173.

794 U.S. National Ice Center (2008, updated daily). *IMS Daily Northern Hemisphere Snow and Ice*
795 *Analysis at 1 km, 4 km, and 24 km Resolutions, Version 1.* NSIDC: National Snow and Ice
796 Data Center. Boulder, Colorado USA. doi: 10.7265/N52R3PMC. Accessed June 9, 2020.

797 Viereck, L. A., and Johnston, W. F. (1990). *Picea mariana* (Mill.) B.S.P. In Burns, R. M. and
798 Honkala, B. H. (eds) *Silvics of North America. Vol. 1. Conifers*, Agricultural Handbook 654,
799 pp. 227–237. U.S. Department of Agriculture, Forest Service.

800 Walter-McNeill, A., Garcia, M. A., Logan, B. A., Bombard, D. M., Reblin, J. S., Lopez, S.,
801 Southwick, C. D., Sparrow, E. L., and Bowling, D. R. (2021). Wide variation of winter-
802 induced sustained thermal energy dissipation in conifers: a common-garden study, *Oecologia*,
803 197(3):589-598.

804 Wang, S., Zhang, L., Huang, C., and Qiao, N. (2017). An NDVI-based vegetation phenology is
805 improved to be more consistent with photosynthesis dynamics through applying a light use
806 efficiency model over boreal high-latitude forests. *Remote Sens.*, 9(7):695.

807 Warren, R. K., Pappas, C., Helbig, M., Chasmer, L. E., Berg, A. A., Baltzer, J. L., Quinton, W.
808 L., and Sonnentag, O. (2018). Minor contribution of overstorey transpiration to landscape
809 evapotranspiration in boreal permafrost peatlands. *Ecohydrology*, 11(5):e1975.

Way, D. A. and Montgomery, R. A. (2015). Photoperiod constraints on tree phenology, performance and migration in a warming world: Photoperiod limits on tree climate responses. *Plant Cell Environ.*, 38(9):1725–1736.

Wold, H. (1975). Path models with latent variables: The NIPALS approach. In Blalock, H. M., Aganbegian, A., Borodkin, F. M., Boudon, R., Capecchi, V. (eds) *International Perspectives on Mathematical and Statistical Modeling: Quantitative Sociology*, pp 307–357. Academic Press.

Wohlfahrt, G. and Gu, L. (2015). The many meanings of gross photosynthesis and their implications for photosynthesis research from leaf to globe. *Plant Cell Environ.*, 38(12):2500–2507.

Wright, S. (1921). Correlation and causation. *J. Agric. Res.*, 20:557–580.

Wu, C., Peng, D., Soudani, K., Siebicke, L., Gough, C. M., Arain, M. A., Bohrer, G., Lafleur, P. M., Peichl, M., Gonsamo, A., Xu, S., Fang, B., and Ge, Q. (2017). Land surface phenology derived from normalized difference vegetation index (NDVI) at global FLUXNET sites. *Agric. For. Meteorol.*, 233:171–182.